ARMA 18–0619

SAND2018-2630C

Acoustic Emission during Borehole Breakout

Choens, R. C.; Ingraham, M. D.; Lee, M. Y.; Yoon, H.; and Dewers, T. A.
Sandia National Laboratories, Albuquerque, New Mexico, USA

This paper was prepared for presentation at the 52nd US Rock Mechanics / Geomechanics Symposium held in Seattle, Washington, USA, 17–20 June 2018. This paper was selected for presentation at the symposium by an ARMA Technical Program Committee based on a technical and critical review of the paper by a minimum of two technical reviewers. The material, as presented, does not necessarily reflect any position of ARMA, its officers, or members. Electronic reproduction, distribution, or storage of any part of this paper for commercial purposes without the written consent of ARMA is prohibited. Permission to reproduce in print is restricted to an abstract of not more than 200 words; illustrations may not be copied. The abstract must contain conspicuous acknowledgement of where and by whom the paper was presented.

ABSTRACT: A novel experimental geometry is combined with acoustic emission monitoring capability to measure crack growth and damage accumulation during laboratory simulations of borehole breakout. Three different experiment are conducted in this study using Sierra White Granite. In the first experiment, the sample is deformed at a constant 17.2 MPa confining pressure without pore fluids; in the second experiment, the sample is held at a constant effective pressure of 17.2 MPa with a constant pore pressure; and in the third experiment, pore pressure is modified to induce failure at otherwise constant stress. The results demonstrate that effective pressure and stress path have controlling influence on breakout initiation and damage accumulation in laboratory simulations of wellbore behavior. Excellent agreement between the dry test and constant pore pressure test verify the application of the effective pressure law to borehole deformation. Located AE events coincide with post-test observations of damage and fracture locations. Comparison of AE behavior between the experiments with pore pressure show that breakouts develop prior to peak stress, and continued loading drives damage further into the formation and generates shear fractures.

1. INTRODUCTION

In subsurface engineering applications, a knowledge of the magnitude and orientation of the in situ stress state is crucial to the success of the project. Stimulated wellbores in unconventional reservoirs must be properly oriented to be successful; tunnels and caverns must account for stress magnitudes to prevent collapse; reservoirs undergoing withdrawal or injection need to maintain a range of effective pressures to prevent formation damage and possible seal breaches; and hazard predictions need the orientation and magnitudes of stresses to predict fault reactivation potential (Cheatham, 1993; Haimson and Herrick, 1986; Marschall et al., 2006; Shamir and Zoback 1992; Zoback et al., 1985; Zoback, 2010). At the surface, there are a number of options available to measure the stress state: flatjacks, overcoring, and anelastic strain recovery (Jaeger et al., 2009). At greater depths in the subsurface, the tight confines of a wellbore or more time intensive process of coring reduce the effectiveness of these methods (Zoback, 2010). The standard way to measure stresses at these depths to use a combination of wellbore tools. Density logs can be integrated to calculated the vertical stress, mini-frac or leak off tests can be used to measure the minimum horizontal stress, and borehole breakouts can be imaged and measured to calculate the maximum horizontal stress (Zoback, 2010). Here, we present experiments using a crystalline rock, Sierra White Granite, to simulate wellbore deformation in the laboratory and better understand the effect of stress path on accumulated damage.

The correct interpretation of borehole breakouts present in wellbores is a crucial step in understanding the state of stress in a formation at depth, and this is the step most prone to errors (JASON, 2014; Zoback, 2010). Integrating density logs and performing leak off test are routine operations with relatively straight forward calculations, leading to reliable estimates of the vertical stress and the minimum horizontal stress. Maximum horizontal stress calculations are based on rock properties and failure behavior, and assumptions about these quantities can lead to errors in stress measurement as high as 30-40% in complicated geologic settings (JASON, 2014). Breakouts are imaged and measured using imaging tools like televiewers or oil based microresistivity imagers, and the width is used to back calculate the stresses necessary to create the observed failure (Barton et al., 1988; Shamir and Zoback, 1992; Vernik and Zoback, 1992; Zoback et al., 1985; Zoback, 2010). Integrated approached incorporating limits based off critically stressed faults and fractures, estimates from dipole sonic logs, and stress drops from observed microseismic events can reduce uncertainties, but borehole breakout measurements remain the standard for estimating the magnitude of the maximum horizontal stress (Zoback, 2010).

Laboratory investigations have utilized two main approaches to understanding wellbore deformation. The first approach utilizes parallelepipeds of rock deformed under a true triaxial stress state, where the maximum principal stress, σ_1, is greater than the intermediate principal stress, σ_2, which is greater than the least

principal stress, σ_3. This experimental technique is fully capable of recreating the stress state at depth, and some apparatus are capable of drilling a borehole under load, recreating the processes that lead to borehole breakouts (Haimson, 2007; Haimson and Herrick, 1986; Labuz and Biolzi, 2007; Lee and Haimson, 1993). However, true triaxial apparatuses are not present in most laboratories, and the tests themselves can be costly and labor intensive. The second approach to simulating wellbore behavior is to use hollow cylinders in a conventional axisymmetric stress state, where σ_1 is greater than $\sigma_2 = \sigma_3$ (Cuss et al., 2003; Dresen et al., 2010; Meier et al., 2015; Salisbury et al., 1991). Conventional load frames are relatively common, samples are easy to prepare, and the frame designs are flexible to allow for a number of variables for investigation. However, this approach cannot apply a differential stress across the simulated wellbore due to the axisymmetric stress state. In this study, we utilize a novel geometry to investigate borehole breakouts in conventional axisymmetric load frames. Modeling the geometry after Kirsch's classic hole in a plate problem, right cylinders of granite have a small hole drilled in the center of the core, perpendicular to the cylindrical axis, to simulate a wellbore. Applying axial stress to the sample creates a differential stress around the wellbore, creating a borehole breakout. Experiments are conducted on Sierra White Granite using two different load paths. The first load path is a standard geomechanics experiment; the sample is deformed at a constant axial strain rate while the effective pressure is held constant. The second load path recreates the drilling environment; the sample is loaded to a high stress state, and the pore pressure is dropped to induce failure. The results show that the experimental geometry recreates borehole breakout behavior in the laboratory. Located AE events coincide with post-test observations of damage. Comparisons of AE behavior with deformed samples demonstrate that breakouts form before peak stress, and the majority of AE is associated with breakout extension into the formation and shear fracture development.

2. METHODS

Experiments were conducted on Sierra White Granite, a granodiorite quarried in California. The samples are medium grained rocks with grain sizes of 1 to 3 mm. The samples are 55-65% plagioclase feldspar, 20-25% quartz, 15-20% orthoclase, 2-4% biotite, 2-4% muscovite, and 1-2% chlorite, with trace amounts of hematite, apatite, zircon, and sphene.

Samples were prepared into 50 mm diameter cylindrical cores, 75 mm in length. Sample ends were treated using a precision surface grinder to ensure parallelism. To simulate wellbore deformation, this study used the Sandia Wellbor Experimental Simulation, SWESI, geometry (Choens et al., 2017). A 11.3 mm hole was drilled into the side of the core, perpendicular to the cylindrical axis and centered along the length of the core. The hole is less than one third the diameter of the core, satisfying Saint-Venant's principle. The stresses along the borehole can be calculated using Kirsch's solutions for a hole in a semi-infinite plate (Kirsch, 1898). According to the solution, loading a hole creates a stress concentration three times greater than the applied stress in the plane perpendicular to the loading direction. Another stress concentration is created on the plane parallel to the loading direction opposite in magnitude to the applied stress (Hubbert and Willis, 1972). The stresses acting along the borehole in the horizontal plane, σ_{BH}, are:

$$\sigma_{BH} = 3 * \sigma_A - P_C - P_P, \quad (1)$$

where σ_A is the axial stress P_C is the confining pressure, and P_P is pore pressure inside the borehole. The stresses along the borehole in the vertical plane, σ_{BV}, are:

$$\sigma_{BH} = 3 * P_C - \sigma_A - P_P. \quad (2)$$

The borehole is isolated from the confining pressure using a machined steel cover. The cover has an inner diameter that corresponds to the core diameter. A high pressure port has been machined into the cover, allowing pore lines to introduce fluids directly into borehole. The covers on both ends of the core have attached pore lines, allowing the boreholes to be filled with fluid and eliminate excess air. A layer of 1.6 mm thick silicon rubber is placed between the cover and the core to help distribute stresses and seat the cover to the core. The cover is affixed using UV cure urethane.

To monitor the evolution of damage during experiments, samples with pore pressure were instrumented with 8 piezoelectric transducers to monitor acoustic emissions, AE. The transducers used in these experiments were Dynasen© piezoelectric pins. The pins were potted into brass fixtures using Wood's metal, and the brass fixtures were mounted to the sample using a quick cure epoxy. The pins were mounted in a diamond and square pattern on either side of the borehole. During testing, AE was monitored and located in real time using a Mistras© Micro-II Express system with an Express-8 eight channel AE board. Signals were preamlified with a 40 dB gain, and bandpass filtered for a range of 150 kHz to 450 kHz. Events were located based on primary threshold crossing. 1 AE hit was recorded when the signal on one channel crossed the 40 dB threshold. 1 AE event was recorded when at least 4 AE hits could be located in the sample.

Friction between steel endcaps and the sample is minimized by coating the endcap faces with a stearic acid – petroleum jelly mix and using a 0.2 mm copper shim in between the endcap and the sample (Labuz and Bridell, 1993). The sample was temporarily affixed to the endcaps using vinyl tape. The samples were isolated from the confining pressure using two applications of a UV cure urethane.

Samples were deformed at 17.2 MPa effective pressure, P_E. A control experiment was performed with a dry borehole at a confining pressure of 17.2 MPa. A constant P_P experiment was performed at 20.6 MPa P_C and 3.4 MPa P_P. Mineral oil was introduced into the borehole after the application of confining pressure. Pore pressure was maintained at a constant value using a syringe pump. Both experiments were conducted at a constant axial strain rate of 3.33×10^{-6} sec^{-1}. Samples were loaded until a plateau in axial stress, at which point the samples were unloaded to prevent the formation of a through-going shear fracture. A third experiment was performed where P_P was lowered under a constant stress to simulate the load path experienced during drilling, the P_P reduction test. The sample was confined at 20.6 MPa P_C and 13.8 MPa P_P. The sample was loaded at a constant axial strain rate of 3.33×10^{-6} sec^{-1} to differential stress, $\Delta\sigma$, of 170 MPa, 85% of the peak stress observed in the dry borehole test. The confining pressure and axial stress was held constant while the P_P was reduced to 3.4 MPa. The sample was held at a constant axial stress and P_E of 17.2 MPa for 2700 seconds.

3. RESULTS

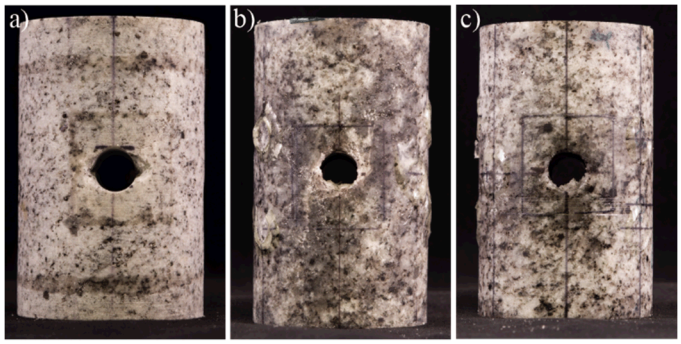

Fig. 1. Deformed samples. a) Dry borehole. b) Constant P_P. c) P_P Reduction.

Deformed samples failed by the development of borehole breakouts running along the length of the borehole for all three experiments (Figure 1). Breakouts formed diametrically opposed on the borehole, oriented perpendicular to the applied axial stress direction. Breakouts have a sharp, dog-eared shape that extend into the formation. Observable fracture growth is limited to the area in the vicinity of the wellbore. Shear fracture extending from the borehole can be observed in the Constant P_P sample; these fractures extend across the diameter of the sample but reduce in size on the other side. The fractures extend downwards on the left side of the borehole and upwards on the right side of the borehole. These fractures are likely incipient shear fractures that would cut across the sample with continued loading. In the P_P reduction test, the damage is higher on the right side of the borehole. For the dry experiment, post-test inspection show no infiltration of confining fluid into the borehole, and saturated boreholes maintained a pressure differential between the confining and pore pressure, indicating that the jacketing and metal cover successfully isolated the borehole.

3.1. Mechanical Results

There is an excellent agreement between the two experiments deformed at a constant axial strain rate (Figure 2, Table 1). Peak differential stress and horizontal borehole stress are nearly identical for the two tests (Table 1). These results indicate that the effective pressure law holds even though the samples were not fully saturated prior to the experiments. The results also show that the inclusion of AE pins on the sample does not affect the sample strength. The loading response is stiffer for the test with pore pressure, but this could reflect the influence of higher confining pressure (Figure 2a). The stress path in differential stress versus mean stress space is identical for the two experiments (Figure 2b).

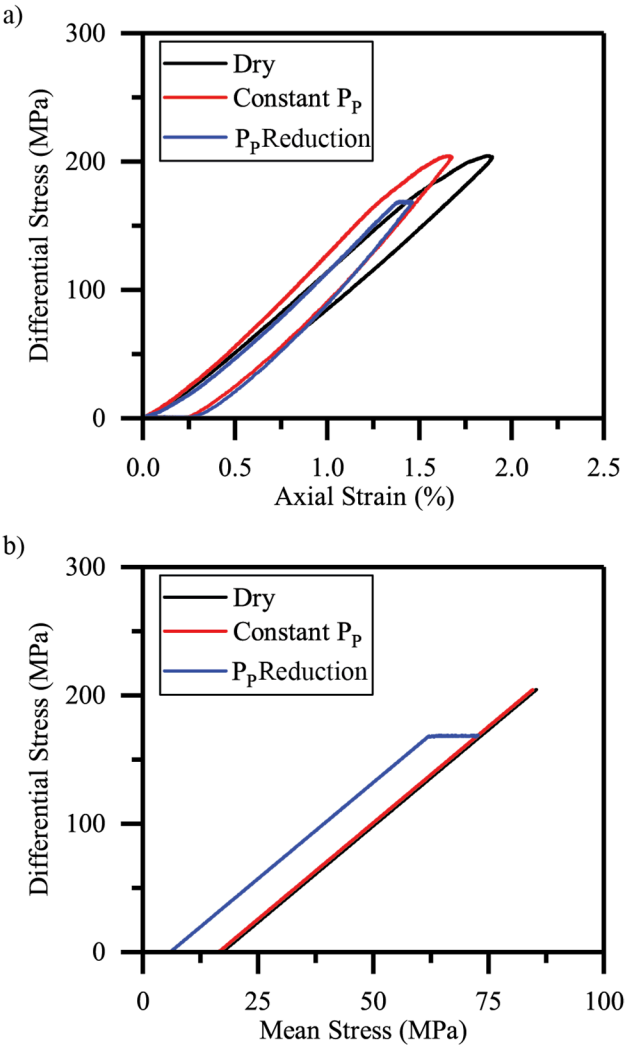

Fig. 2. Mechanical results from simulated borehole deformation experiments. a) Differential stress versus strain. b) Stress paths in differential stress versus mean stress space.

Table 1. Peak Strength and measured AE

Test	$\Delta\sigma$ (MPa)	σ_{BH} (MPa)	AE Hits	AE Events
Dry	204.7	648.5	---	---
Constant P_P	204.5	649.7	92438	2215
Dropping P_P	169.2	543.8	24751	856

The P_P Reduction test was held at a constant stress level for 1110 seconds while the pore pressure was reduced, and held for an additional 2700 seconds once the pore pressure reached 3.4 MPa. During this time interval, the sample strained by 0.1%. After the reduction in pore pressure, the creep level was 85% of the peak strength from the dry test and Constant P_P test. The loading stiffness of the P_P Reduction sample is initially softer than the Constant P_P and dry borehole samples, but the P_P Reduction sample appears to stiffen with increased loading to have a similar response to the Constant P_P after 125 MPa differential stress.

3.2. *Acoustic Emission Data*

There are large differences in observed AE activities between the Constant P_P test and the P_P Reduction test (Figure 3, Table 1). The P_P Reduction test has only 26% of the AE hits and 39% of located AE events as compared to the Constant P_P test.

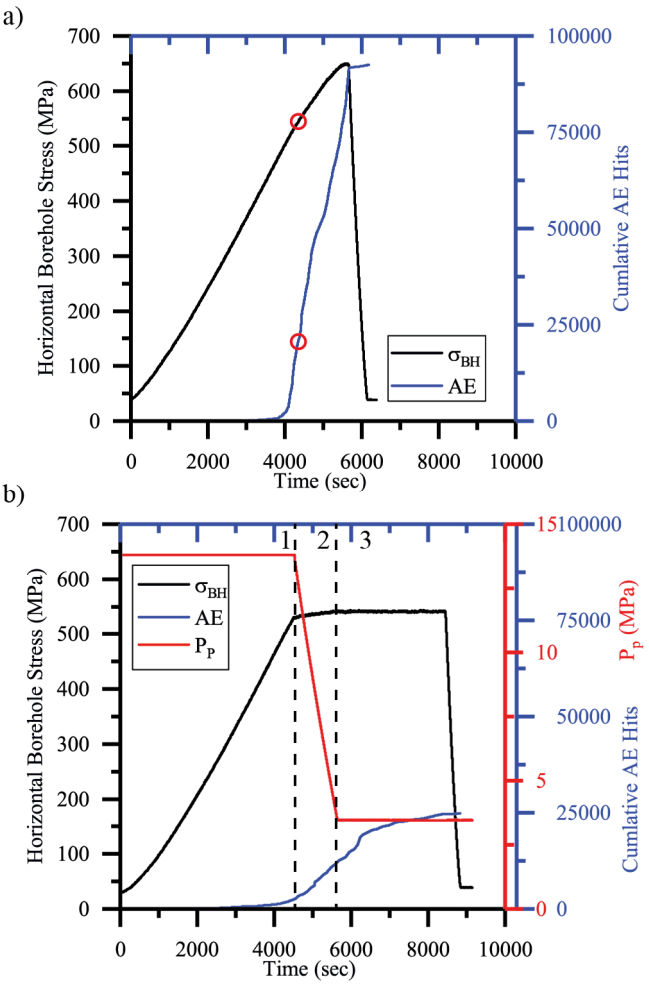

Fig. 3. a) σ_{BH} and AE versus time for Constant P_P test. Red circle mark stess level from P_P Reduction test and corresponding AE level. b) σ_{BH}, pore pressure, and AE versus time for P_P Reduction test. Stages of P_P annotated. 1 Loading at constant pore pressure, 2 dropping pore pressure, and 3 creep at constant pore pressure.

In the Constant P_P test, negligible AE events are seen during the initial stage of loading. At approximately 60% of the peak load, there is an observable onset in AE activity. At approximately 80% of the peak load, there is rapid increase in AE activity that continues until unloading (Figure 3a). The steep and constant slope of AE hits with time reflect saturation of acquisition hardware.

Located AE events are grouped in two clusters in the center of the sample on either side of the simulated wellbore (Figure 4a). AE events originally cluster horizontally around the sample, and there is vertical migration away from the borehole after 5000 seconds. At this time, the sample is close to peak stress. Events are distributed evenly along the length of the wellbore (Figure 4b, c). Some AE events are mislocated to the empty space of the borehole, likely due to reflections of raypaths off the borehole.

In the P_P Reduction test, the onset of AE occurs during the intial loading stage of the experiment (Figure 3b). There is an increase in AE, but axial stress is held constant before AE can surge like that observed in the Constant P_P test (Figure 3a). AE continues at a constant rate during the second stage of the experiment as the pore pressure drops. AE continues into the third stage of the experiment, where the sample is allowed to creep at a higher P_E. 500 seconds into the creep phase, or after 6100 seconds total, there is a sharp jump in number of AE hits (Figure 3b). After this jump, AE starts to taper off with time.

AE events are grouped in two cluster in the center of the sample around the borehole, but the distribution is not equal between the two sides as more events are located on the right side of the borehole (Figure 5a). Events are distributed evenly along the length of the borehole (Figure 5b, c). AE events are preferentially occurring on the right side of the core after 5000 seconds, but the surge in AE that occur between 6000 and 7000 seconds is highly asymmetric. These events occur overwhelmingly on the right side of the core, concentrated towards the front of the borehole (Figure 5a, b).

4. DISCUSSION AND CONCLUSIONS

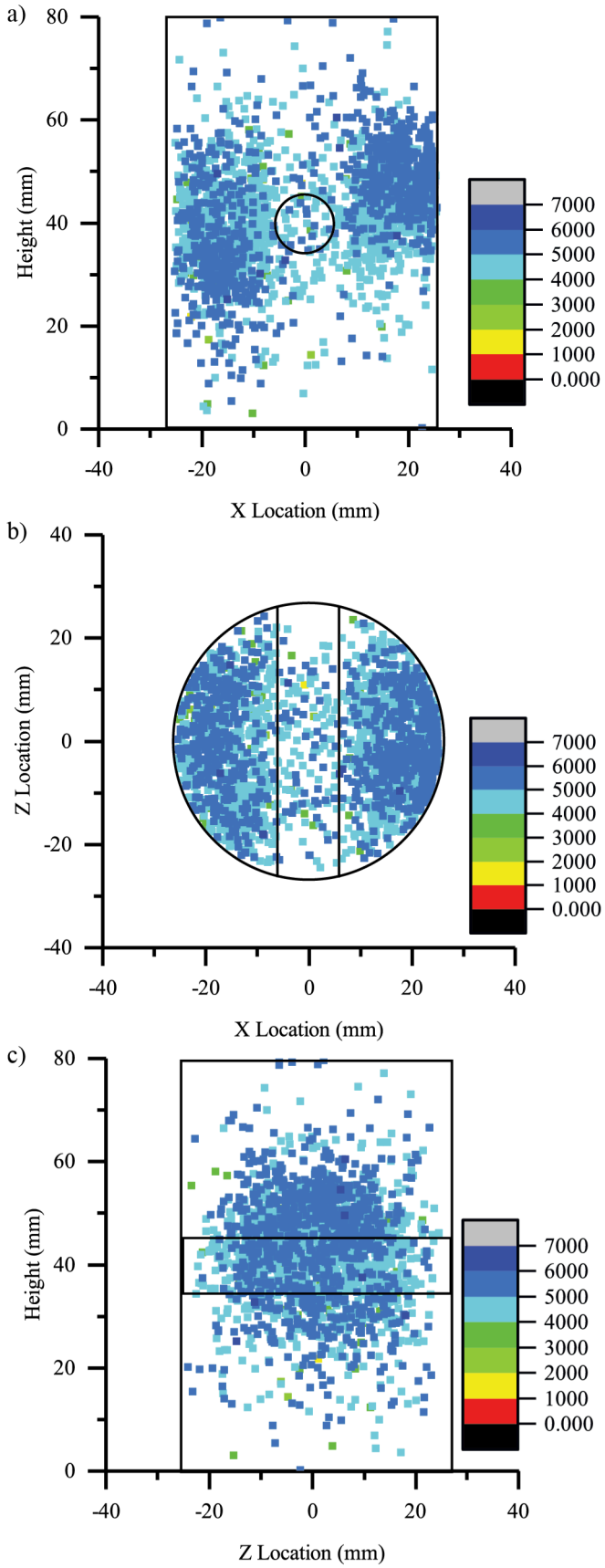

Fig. 4. Located events for Constant P_P test. a) Vertical distribution of AE event around the borehole. b) Map view of AE events. c) Vertical distribution of AE events along the borehole.

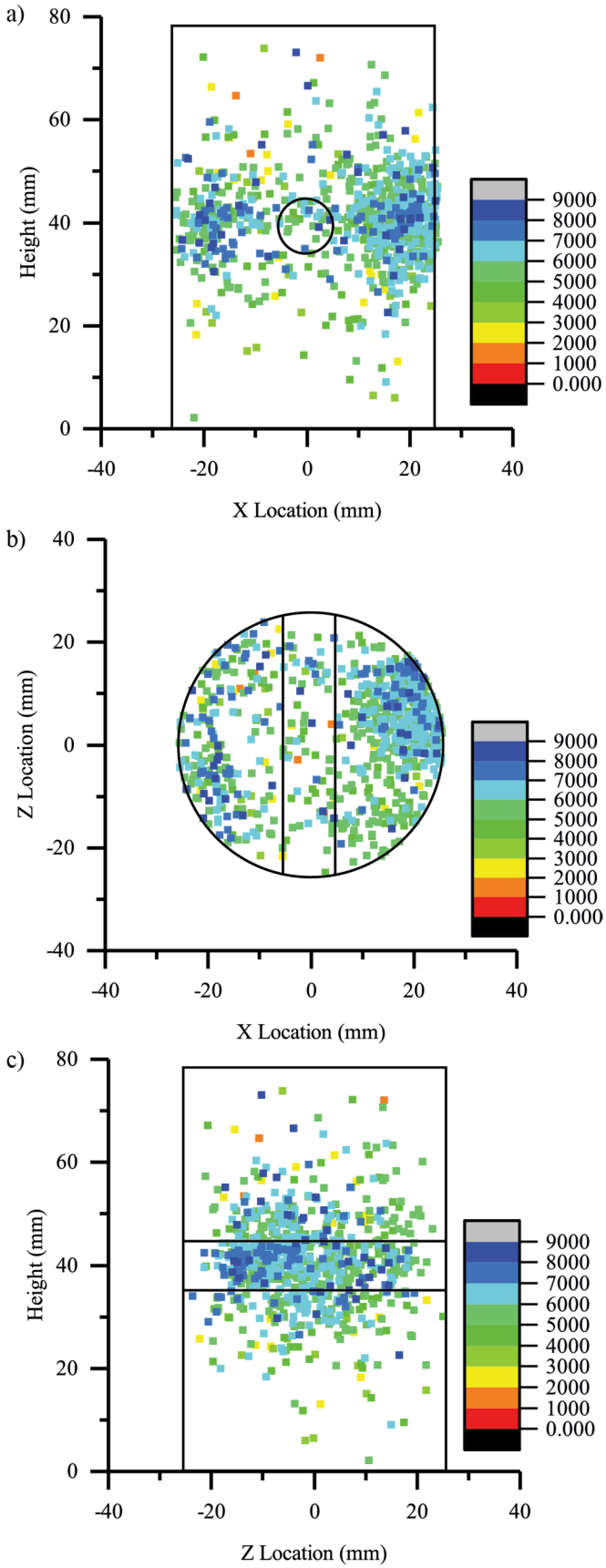

Fig. 5. Located events for Constant P_P test. a) Vertical distribution of AE event around the borehole. b) Map view of AE events. c) Vertical distribution of AE events along the borehole.

The similarity of the mechanical results for the dry borehole test and the Constant P_P test suggest that the effective pressure law holds for these tests. The samples have identical peak stresses for 17.2 MPa P_C and 17.2 MPa P_E. The borehole fluid is mineral oil, a non-wetting fluid that should not trigger chemical reactions in the rock at the temperatures and timescales of these tests. These results also indicate that the failure must occur at the borehole interface. The samples are not saturated prior to deformation; mineral oil is introduced into the borehole after the sample is under confinement. The mineral oil does not have a chance to penetrate far into the formation due to its thick viscosity and Sierra White Granite's low porosity and permeability. The pore pressure should only equilibrated in the vicinity of the borehole. Failure must initiate near the borehole for the peak stress to agree with the dry borehole test. As fracture form near the wellbore, the permeability should increase and with it the extent of pore pressure penetration into the sample.

Located AE events coincide with post-test observations of the samples. In the Constant P_P test, there is a vertical migration of AE events away from the borehole after 5000 seconds (Figure 4a). On the left side of the borehole, the cloud of events is migrating downwards, and on the right side of the borehole, the cloud is migrating upwards. These patterns match the observed fractures extending away from the borehole, indicating the development of these fractures is responsible for the AE migration (Figure 1b). The AE events help to constrain the timing of the shear fractures, as they must have developed after 5000 seconds. In the P_P Reduction test, AE events localize on the right side of the borehole closer to one end after 6000 seconds. This pattern matches the observed post-test deformation of the sample, also constraining timing on fracture development. The agreement between located AE events and observed deformation supports the accuracy of the Mistras© software localization algorithm. Some AE events are mislocated by the software, e.g. events located inside the borehole, but further refinements to the velocity model could reduce discrepancies.

There is a substantial difference in the total number of AE hits observed in the Constant P_P test and the P_P Reduction test; the observed number of AE hits in the Constant P_P test is 373% of that observed in the P_P Reduction test, with only an additional 15% loading increment (Table 1). Despite the large difference in total AE hits, there is good agreements between the tests. The cumulative hits in the Constant P_P test at 85% load is around 21,000 hits (Figure 3a). Comparatively, the P_P Reduction test has more hits for the same stress level, most likely due to the extended creep stage. The good agreement between the observed AE at the same stress level indicate that the active deformation mechanisms are similar between the different stress paths. In post-test observations of the P_P Reduction test, borehole breakouts are well defined and traverse the length of the sample. This suggest that in the Constant P_P test conducted at a constant axial strain rate, the breakouts are formed in the sample before the occurrence of peak stress. The sharp increase in AE after 4000 seconds most likely corresponds to the initiation of breakouts in the sample, and the majority of subsequent AE represent damage associated with increasing breakout size and the development of shear fractures (Figure 1, 3, 4a).

The tests conducted in this study demonstrate the versatility of our experimental geometry to investigate wellbore deformation phenomena. This geometry successfully recreates borehole breakouts in the laboratory using standard geomechanics load frames. Tests were conducted dry and with pore pressure, and the results show the effective pressure law holds in the borehole environment despite the tight crystalline rock and viscous pore fluid employed in this study. Peak stress is identical between the dry borehole and Constant P_P test. Located AE events demonstrate that deformation clusters around the borehole where breakouts form, and track the development of damage and shear fractures. Comparisons between post-test deformation in the P_P Reduction sample and the AE activity in the Constant P_P test show that breakouts initiate prior to failure, and continued loading increases damage in the formation with increasing fracture development.

The authors would like to thank Michelle Williams, Aron Robbins, and Eric Robbins for assistance in specimen preparation, and in performing tests. Funding for this work was provided by Sandia National Laboratories: Laboratory Directed Research and Development program. Sandia National Laboratories is a multimission laboratory managed and operated by National Technology and Engineering Solutions of Sandia LLC, a wholly owned subsidiary of Honeywell International Inc. for the U.S. Department of Energy's National Nuclear Security Administration under contract DE-NA0003525.

REFERENCES

Barton, C. A., Zoback, M. D., and Burns K. L. (1988). In-situ stress orientation and magnitude at the Fenton Geothermal Site, New Mexico, determined from wellbore breakouts. *Geophysical Research Letters, 15*(5), 467-470, doi:10.1029/GL015i005p00467.

Cheatham, J. (1993). A new hypothesis to explain stability of borehole breakouts. *International Journal of Rock Mechanics and Mining Sciences & Geomechanics Abstracts 30*(7), 1095-1101.

Choens, R. C., Ingraham, M. D., Lee, M. Y., Dewers, and T. A. (2017). *Novel experimental techniques to*

investigate wellbore damage mechanisms. Presented at The AGU Fall Meeting, New Orleans, LA.

Cuss, R., Rutter, E., and Holloway R. (2003). Experimental observations of the mechanics of borehole failure in porous sandstone. *International Journal of Rock Mechanics and Mining Sciences, 40*(5), 747-761.

Dresen, G., Stanchits, S., and Rybacki E. (2010). Borehole breakout evolution through acoustic emission location analysis. *International Journal of Rock Mechanics and Mining Sciences, 47*(3), 426-435.

Jaeger, J. C., Cook, N. G., and Zimmerman R. (2009). *Fundamentals of rock mechanics*, Hoboken, NJ: John Wiley.

JASON, The MITRE Corporation. (2014). *Subsurface Characterization Letter Report* (JSR-14-Task-013). McLean, VA.

Haimson, B. C. (2007). Micromechanisms of borehole instability leading to breakouts in rocks. *International Journal of Rock Mechanics and Mining Sciences, 44*(2), 157-173.

Haimson, B. C., and Herrick C. G. (1986). *Borehole breakouts-a new tool for estimating in situ stress?* Paper presented at International Symposium on Rock Stress and Rock Stress Measurements, Stockholm, Sweden.

Hubbert, M. K., and Willis, D. G. (1972). *Mechanics of Hydraulic Fracturing* (T.P. 4597). Paper presented at Petroleum Branch Fall Meeting, Los Angeles, CA.

Kirsch, E. G. (1898). Die Theorie der Elastizit t und die Bed rfnisse der Festigkeitslehre. *Zeitshrift des Vereines deutscher Ingenieure 42*(1), 797-807.

Labuz, J. F., and Biolzi L. (2007)., Experiments with rock: remarks on strength and stability issues. *International Journal of Rock Mechanics and Mining Sciences, 44*(4), 525-537.

Labuz, J. F., and Bridell J. (1993). Reducing frictional constraint in compression testing through lubrication. *International Journal of Rock Mechanics and Mining Sciences and Geomechanics, 30*(4), 451-455.

Lee, M. Y., and Haimson B. (1993). Laboratory study of borehole breakouts in Lac du Bonnet granite: a case of extensile failure mechanism. *International Journal of Rock Mechanics and Mining Sciences & Geomechanics Abstracts, 30*(7), 1039-1045.

Marschall, P., Distinguin, M., Shao, H., Bossart, P., Enachescu, C., and Trick T. (2006), *Creation and evolution of damage zones around a microtunnel in a claystone formation of the Swiss Jura Mountains* (SPE 98537). Paper presented at SPE International Symposium and Exhibition on Formation Damage Control, Lafayette, LA.

Meier, T., Rybacki, E., Backers, T., and Dresen G. (2015.), Influence of bedding angle on borehole stability: a laboratory investigation of transverse isotropic oil shale. *Rock Mechanics and Rock Engineering, 48*(4), 1535-1546.

Salisbury, D., Ramos, G., and Wilton B. (1991). *Wellbore instability of shales using a downhole simulation test cell*. Paper presented at The 32nd US Symposium on Rock Mechanics (USRMS), Norman, OK.

Shamir, G., and Zoback M. D. (1992). Stress orientation profile to 3.5 km depth near the San Andreas fault at Cajon Pass, California. *Journal of Geophysical Research, 97*(B4), 5059-5080.

Zoback, M. D. (2010). *Reservoir geomechanics,* Cambridge, UK: Cambridge University Press.

Zoback, M. D., Moos, D., Mastin, L., and Anderson, R. N. (1985). Well bore breakouts and in situ stress. *Journal of Geophysical Research, 90*(B7), 5523-5530.

Vernik, L., and Zoback M. D. (1992). Estimation of maximum horizontal principal stress magnitude from stress induced well bore breakouts in the Cajon Pass Scientific Research borehole. *Journal of Geophysical Research, 97*(B4), 5109-5119.